

Learning Rich Features for Gait Recognition by Integrating Skeletons and Silhouettes

Yunjie Peng, Saihui Hou, Kang Ma, Yang Zhang, Yongzhen Huang, Zhiqiang He*

Abstract—Gait recognition captures gait patterns from the walking sequence of an individual for identification. Most existing gait recognition methods learn features from silhouettes or skeletons for the robustness to clothing, carrying, and other exterior factors. The combination of the two data modalities, however, is not fully exploited. This paper proposes a simple yet effective *bimodal fusion (BiFusion) network*, which mines the complementary clues of skeletons and silhouettes, to learn rich features for gait identification. Particularly, the inherent hierarchical semantics of body joints in a skeleton is leveraged to design a novel *Multi-scale Gait Graph (MSGG) network* for the feature extraction of skeletons. Extensive experiments on CASIA-B and OUMVLP demonstrate both the superiority of the proposed MSGG network in modeling skeletons and the effectiveness of the bimodal fusion for gait recognition. Under the most challenging condition of walking in different clothes on CASIA-B, our method achieves the rank-1 accuracy of 92.1%. The code will be released at <https://github.com/YunjiePeng/BimodalFusion> after the acceptance.

Index Terms—Gait recognition, Biometrics, Graph convolutional network (GCN), Convolutional neural network (CNN).

I. INTRODUCTION

GAIT recognition measures unique physical and behavioral characteristics from the walking pattern of an individual for identification [1]. Compared with other biometrics such as the face [2], fingerprint [3], and iris [4], gait can be identified at a distance without the cooperation of target subjects. It has broad applications in crime prevention, forensic identification, and social security [5], [6]. However, the exterior factors such as clothing, carrying condition, and camera viewpoints greatly change the gait appearance and bring significant challenges to gait recognition.

To alleviate the issue, various methods have been proposed and can be roughly categorized into RGB-based, event-based, silhouette-based, and skeleton-based methods according to the input data modality. The RGB-based methods [7], [8] usually employ generative networks or skinned multi-person linear (SMPL) models to filter out color and texture information

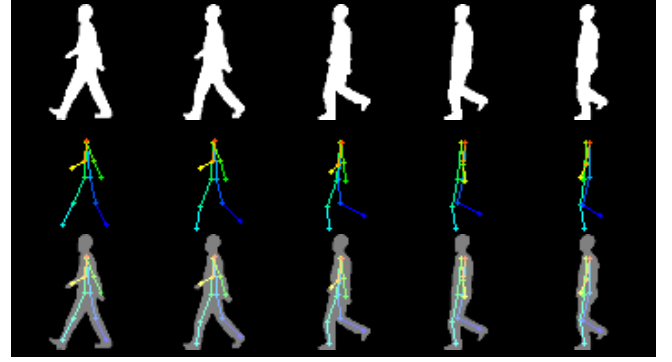


Fig. 1. The overlapping of limbs and torso in silhouettes during walking (first row). The skeletons of the same walking sequence (second row). Visually, the combination of skeletons and silhouettes (third row) retains both the external outline and the articular structure simultaneously. It is expected to be a more comprehensive representation for gait.

from the raw RGB images for identification. These methods are facing the challenge of discarding irrelevant information for gait and require cross-dataset experiments to validate the effectiveness. The event-based methods [9] are proposed with the development of event cameras. Event cameras capture event streams at each pixel and have the advantages of ultra-low resources consumption and high temporal resolution [10]. Nevertheless, noisy and asynchronous event streams are relatively hard to deal with.

The silhouette-based and skeleton-based methods are the two most competitive gait recognition methods in the research community. The silhouette-based methods [11]–[13] extract features from silhouette sequences to eliminate the impact of exterior factors. These methods are suitable for low-resolution conditions and have achieved state-of-the-art (SOTA) results on public gait datasets. Despite the superiority, further improvements of these methods are limited: the silhouette only retains the external outline; some body parts information is lost due to the *overlapping* of limbs and torso during walking, as shown in Fig. 1. The skeleton-based methods [14]–[16] perform human pose estimation [17], [18] first and capture gait patterns from skeleton sequences for recognition. The skeleton well preserves the body structure information but ignores the discriminative body shape information, resulting in the poor performance of skeleton-based methods.

While the silhouette retains the body shape information and omits some body part clues, the skeleton preserves the body structure information and ignores the shape instead. The two data modalities are complementary to each other and their combination is expected to be a more comprehensive repre-

*Corresponding author.

Yunjie Peng is with the School of Computer Science and Technology, Beihang University, Beijing 100191, China (email: yunjiapeng@buaa.edu.cn).

Saihui Hou and YongZhen Huang are with the School of Artificial Intelligence, Beijing Normal University, Beijing 100875, China (email: housaihui@bnu.edu.cn; huangyongzhen@bnu.edu.cn).

Kang Ma is with the Watrix Technology Limited Co. Ltd., Beijing, China (email: xkangma@gmail.com).

Yang Zhang is with the Smart Education Lab, Lenovo Research, Beijing, China (email: zhangyang20@lenovo.com).

Zhiqiang He is with the School of Computer Science and Technology, Beihang University, Beijing 100191, China and the Lenovo Corporation, Beijing, China (email: zqhe1963@gmail.com).

sensation for gait. However, the complementary strengths of skeletons and silhouettes are not fully exploited in the previous literature. As far as we know, the early work proposed by Boulgouris et al. [19] only considered employing the skeleton structure defined by human anatomy as a body component locator to assist the local feature extraction of silhouettes. The holistic and local silhouette features of automatically labeled components under the left side-view are combined through a pair of Hidden Markov Models for gait recognition. In this way, the more discriminative gait patterns contained in the motion of a skeleton sequence are ignored.

To fully mine the complementary clues and avoid losing the crucial discriminative information retained in either of the two data modalities, we propose a simple yet effective *bimodal fusion (BiFusion) network* which separately exploits the skeletons and silhouettes. Specifically, we adapt the widely-used graph convolution network (GCN) for the graph-structured skeleton data. The inherent hierarchical semantics of body joints in a skeleton is leveraged to design a novel *Multi-scale Gait Graph (MSGG) network* for the feature extraction of skeletons. And the part-based feature-level fusion is applied on features extracted from silhouettes and skeletons to exploit the complementary strengths of the two data modalities for effective gait identification.

In summary, the major contributions of this work lie in three aspects:

- We propose a novel *Multi-scale Gait Graph (MSGG) network* which can automatically capture the gait patterns from the raw skeleton data in a hierarchical manner.
- We fully exploit the *complementary strengths* of the two data modalities, i.e., skeletons and silhouettes, and design a simple yet effective *bimodal fusion (BiFusion) network* for gait recognition.
- Experiments on CASIA-B and OUMVLP demonstrate both the superiority of the proposed MSGG network among skeleton-based methods and the effectiveness of the bimodal fusion in gait identification.

II. RELATED WORK

A. Silhouette-based Gait Recognition

The silhouette-based methods can be roughly divided into three categories according to the way they deal with the temporal information. The first category [20]–[22] regards gait as a template and compresses the silhouettes into an image for identification, e.g. Gait Energy Image (GEI) or Gait Entropy Image (GEnI). Despite the simplicity, these methods inevitably lose fine-grained temporal and spatial information. The second [23]–[25] regards gait as a video sequence and employs the LSTM-based or 3D-CNN-based model to extract temporal patterns. These models can capture rich temporal information but require higher computational cost and are relatively hard to train. The third category [11]–[13] regards gait as an unordered set and applies statistical functions to aggregate the temporal information along the set dimension. It has achieved significant improvements and becomes popular among the research community recently for both simplicity and effectiveness.

In this work, we treat the silhouette sequence as an unordered set and directly employ the GaitPart [12] as the silhouette module of the proposed bimodal fusion network. In GaitPart, the authors observe that different parts of a human body have evidently various visual appearances and moving patterns during walking. Based on the multiple parts obtained by horizontally splitting a feature map, the GaitPart learns personalized spatial-temporal representation for each part through the separate 2D convolution operation and the micro-motion extraction on different parts across frames, i.e., the Focal Convolution Layer and the Micro-motion Capture Module in GaitPart [12].

B. Skeleton-based Gait Recognition

The raw skeleton data predicted by pose estimation methods is not in the form of regular 2D or 3D grids and extra handcrafted formulations or rules are required for traditional skeleton-based methods [14], [26]. For instance, PoseGait [14] defines three kinds of spatial-temporal pose features (i.e., joint angle, joint motion, and limb length) based on human prior knowledge and rearranges them to form a feature matrix as the input of a CNN-based model for identification. These methods rely on handcrafted input features which makes the whole process complex and sub-optimal. Differently, the recent skeleton-based methods [15], [16], [27] propose to adapt the GCN for automatically modeling the graph-structured skeleton data. Benefiting from the powerful graph modeling capability of the GCN, these methods have made significant improvements in skeleton-based gait recognition.

To a certain degree, the skeleton-based GCN methods are closely related to the ST-GCN [28]. The spatial-temporal graph of ST-GCN is widely adopted due to the ability of modeling variable-length skeleton sequences. However, the whole architecture of the spatial-temporal graph is inherently flat and the lack of hierarchy structure is especially problematic due to the global pooling operation on the embeddings of all nodes to get an entire graph representation. Therefore we propose to leverage the inherent hierarchical semantics of body joints in a skeleton and construct a 3-scale hierarchical network named *MSGG* which can aggregate complex multi-scale information for gait recognition. It is worth noting that the multi-scale GCN is first proposed in CTL [29] for video-based person re-identification and the MSGG differs from it in three aspects. First, CTL deals with local RGB features extracted (located) by the pose estimation method while the MSGG directly processes the raw skeleton data. Second, the multi-scale skeleton graph defined by CTL is based on human anatomy while that of MSGG is defined by the moving trend of each joint during walking. Third, CTL performs multi-layer 3D graph convolution on different body partition scales separately while the MSGG passes information across scales after every spatial-temporal convolution within each scale.

C. Multimodal Biometric Fusion

Two or more data modalities are employed to extract and combine relevant information for identification in multimodal biometric fusion [30], [31]. Generally, multimodal fusion can

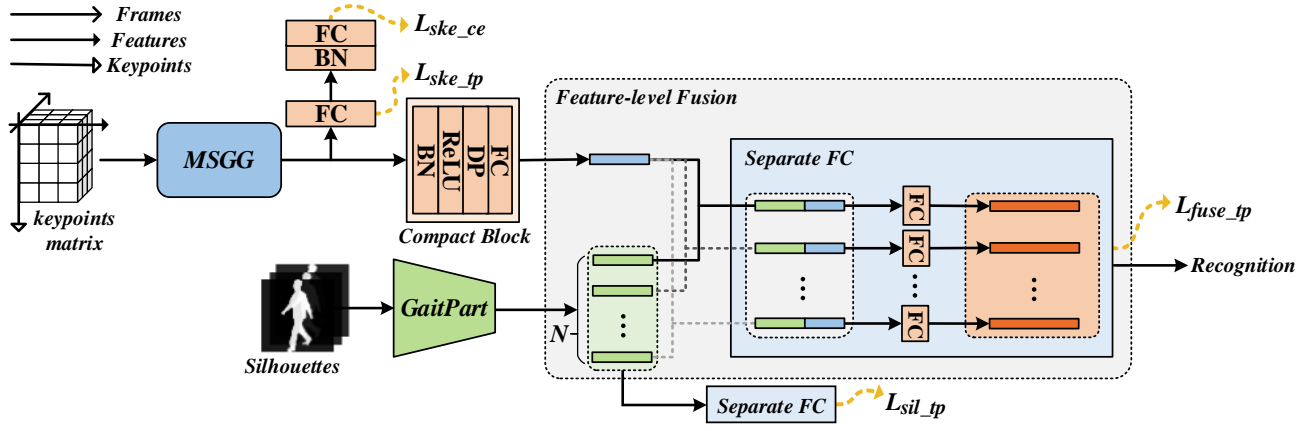


Fig. 2. The overall architecture of our proposed bimodal fusion network. The GaitPart module extracts N part features from the silhouettes. The MSGG module takes the predicted keypoints matrix as input and captures gait patterns from the skeletons. BN for *Batch Normalization*, DP for *Dropout*, and FC for the *Fully Connected Layer*. Separate FC denotes for N FCs performed on N fusion features separately.

be classified into data-level, feature-level, and decision-level fusion according to the level at which the fusion is done. Compared with data-level and decision-level fusion, feature-level fusion preserves raw information of different modalities and is expected to reach better results [32]–[34]. In practice, feature-level fusion has been applied in a number of multi-modal biometric identification tasks. For instance, Bodla et al. [30] propose a heterogeneous feature fusion network to concatenate both the raw features and the non-linear projected features obtained from two different pre-trained deep CNNs for template-based face recognition. Another example is that Yang et al. [35] combine face, fingerprint, and finger vein fisher vector features in series and project the fused feature for multimodal person identification.

Motivated by the complementary strengths of the silhouettes and skeletons, we adopt feature-level fusion to learn rich features from the two data modalities for effective gait identification.

III. PROPOSED METHOD

In this work, we propose a bimodal fusion network to exploit the complementary strengths of different data modalities for gait recognition. The overall architecture of the proposed bimodal fusion network is shown in Fig. 2.

A. Pipeline Overview

The complementary strengths of the two data modalities, i.e., silhouettes and skeletons, motivate us to fuse them and exploit their relevant information for gait recognition. Specifically, we directly employ the GaitPart [12] for the silhouette data and design a novel *Multi-scale Gait Graph (MSGG)* network to hierarchically aggregate the multi-scale information for the skeleton data. The part-based feature-level fusion is applied to combine different data modalities for identification.

Formally, given a dataset of P people with identities p_i , $i \in \{1, 2, \dots, P\}$, we denote the silhouette sequence and the

*keypoints matrix*¹ generated from a walking sequence of p_i as S_i and K_i , respectively. The proposed network obtains gait features from the bimodal fusion of S_i and K_i through 3 steps, formulated as:

$$k_i = \text{CmpB}(\text{MSGG}(K_i)) \quad (1)$$

$$s_i^1, s_i^2, \dots, s_i^N = \text{GaitPart}(S_i) \quad (2)$$

$$f_i^n = \text{Fuse}_n(s_i^n, k_i), \quad n = 1, 2, \dots, N \quad (3)$$

where the *MSGG* generates the skeleton sequence features from the *keypoints matrix* K_i and the *GaitPart* extracts N part-based features from the silhouette sequence S_i . Further details about the GaitPart can be found in Sec. II-A. The skeleton-based MSGG module will be introduced in Sec. III-B. The Compact Block [13] is applied to get the compact features k_i for skeletons, abbreviated as *CmpB* in Eq. 1. The structure of the Compact Block is clearly illustrated in Fig. 2. The function Fuse_n aims to extract specialized information from the compact skeleton sequence features k_i for the n -th silhouette sequence part features s_i^n and obtains the proper fusion features f_i^n for gait identification. Further details about the Fuse_n are illustrated in Sec. III-C.

B. Multi-scale Gait Graph Network

The proposed *Multi-scale Gait Graph (MSGG)* network constructs a pyramid spatial-temporal graph on skeletons with semantics going from shallow to deep. The information can then be hierarchically aggregated by MSGG for identification.

Pyramid Spatial-Temporal Graph Construction. As shown in Fig. 3 (a), the pyramid spatial-temporal graph consists of three subgraphs corresponding to three scales, namely the *joints*, the *limbs*, and the *bodyparts* spatial-temporal graph. (1) The *joints* spatial-temporal graph is constructed with the joints of skeletons as graph nodes, the natural connectivities

¹The *keypoints matrix* is a 3D matrix that organizes the skeleton sequence data into regular grid formats. Each keypoint in a skeleton contains three initial features, i.e., the x , y coordinates of the keypoint in the frame and the confidence of the prediction.

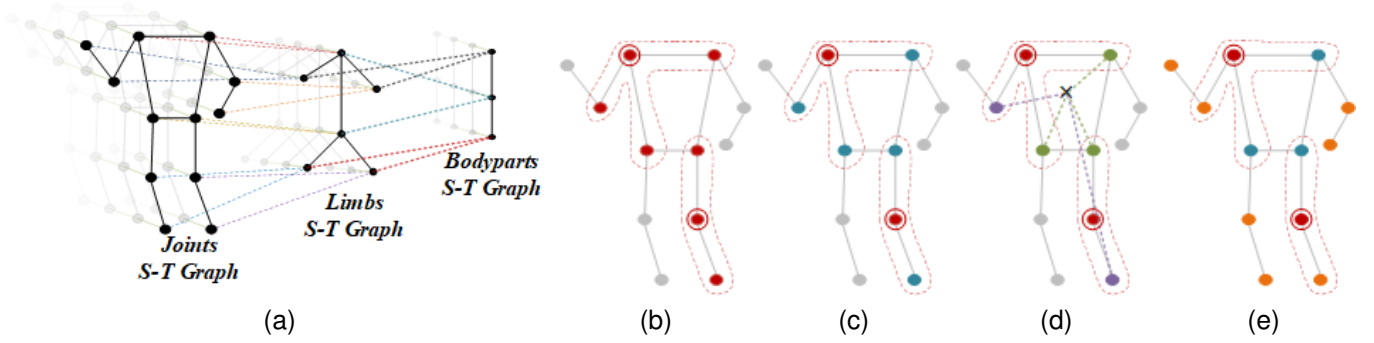


Fig. 3. (a) The proposed pyramid spatial-temporal graph. *S-T* stands for spatial-temporal. (b) *Uniform labeling*: all nodes in a neighborhood have the same label. (c) *Distance partitioning*: nodes in a neighborhood are divided into two subsets (red and blue) by the distance between the current node and the root node (red). (d) *Spatial configuration partitioning*: nodes are labeled into three subsets (red, green, and purple) according to their distances to the gravity center (gray cross) compared with that of the root node (red). (e) *Gait temporal partitioning*: nodes are divided into three subsets (red, blue, and orange) where neighbor nodes of the root node (red) are divided into two subsets (blue and orange) according to their moving amplitudes.

in human bodies as spatial edges, and the connections of the same joints across the adjacent frames as temporal edges. (2) The *limbs* spatial-temporal graph is constructed on the *joints* spatial-temporal graph by pooling every two joints of a limb in the same frame into one node. The reason for this is that the two joints of a limb can represent a physically rigid body in which the same moving trend is shared. (3) The *bodyparts* spatial-temporal graph is constructed on the *limbs* spatial-temporal graph by pooling every two nodes of a body part in the same frame into one node. The higher-level semantic meaning is reached through grouping the nodes of limbs into corresponding body parts, i.e., torso, arms, and legs.

Subgraph Information Aggregation. Before diving into the information aggregation on the whole pyramid spatial-temporal graph, we first look at that within each subgraph, i.e., the joints, the limbs, or the bodyparts spatial-temporal graph. Given a skeleton sequence with T frames and N nodes per frame, the subgraph is denoted as $G = (V, E)$. The node set $V = \{v_{ti} | t = 1, 2, \dots, T, i = 1, 2, \dots, N\}$ and the edge set $E = \{E_{temporal} \cup E_{spatial}\}$, where $E_{temporal} = \{(v_{ti}, v_{t+1i}) | t = 1, 2, \dots, T-1, i = 1, 2, \dots, N\}$ contains inter-frame edges which connect the same nodes in consecutive frames and $E_{spatial} = \{(v_{ti}, v_{tj}) | (i, j) \in H\}$ includes intra-frame edges which depict the natural connectivities in a human body based on H . H is a set of connected nodes within a human body defined by the corresponding subgraph in Fig. 3 (a). The information aggregation on G consists of two alternatively performed steps: (a) the spatial information aggregation on nodes in a single frame and (b) the temporal information aggregation on the same node across the adjacent frames, which are elaborated as the follows.

(a) *Spatial Information Aggregation.* We adopt the implementation of the graph convolution in ST-GCN [28] to aggregate the spatial information for each frame. Given the spatial graph $G_t = (V_t, E_{spatial}^t)$ and the input feature matrix f_{in}^t at the t -th frame, the spatial graph convolution is formulated as:

$$f_{out}^t = \Lambda^{-\frac{1}{2}}(A + I)\Lambda^{\frac{1}{2}}f_{in}^t W \quad (4)$$

where A and I are adjacency matrix and identity matrix of G_t . The degree matrix Λ is calculated by $\Lambda^{ii} = \sum_j (A^{ij} + I^{ij})$.

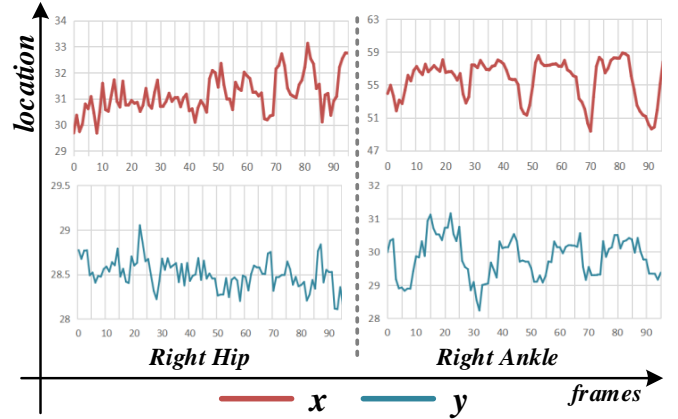


Fig. 4. Location changes of the right hip and the right elbow on the aligned skeleton sequence along the x -axis and the y -axis, respectively. The joints with larger amplitudes of movement (e.g. the right ankle) are more likely to retain the gait periodicity than the joints with smaller amplitudes of movement (e.g. the right hip).

Nodes can aggregate information from neighbors with Eq. 4, where W is a trainable weight transform matrix.

In essence, the above formula directly sums the features of a neighbor set $N(v_{ti}) = \{v_{tj} | d(v_{ti}, v_{tj}) \leq 1\}$, where $d(v_{ti}, v_{tj})$ denotes the shortest path from v_{ti} to v_{tj} , as the output feature for the node v_{ti} . To improve the expressiveness of the spatial graph convolution, we partition the neighbor set $N(v_{ti})$ of node v_{ti} into a fixed K subsets and propagate the information for each subset separately. Here we define the mapping $l_{ti} : N(v_{ti}) \rightarrow \{0, 1, \dots, K-1\}$ which maps a node in the neighbor set $N(v_{ti})$ to its subset label. The spatial graph convolution with K subsets is formulated as:

$$f_{out}^t = \sum_{k=1}^K \Lambda_k^{-\frac{1}{2}}(A_k + I)\Lambda_k^{\frac{1}{2}}f_{in}^t W_k \quad (5)$$

where $\Lambda_k^{-\frac{1}{2}}(A_k + I)\Lambda_k^{\frac{1}{2}}$ denotes the normalized adjacency matrix and W_k denotes a trainable weight transform matrix for the k -th subset of each neighbor set on graph G_t , respectively.

(a1) *Partition Strategy.* Given the formulation of graph convolution in Eq.5, it is important to design a proper node

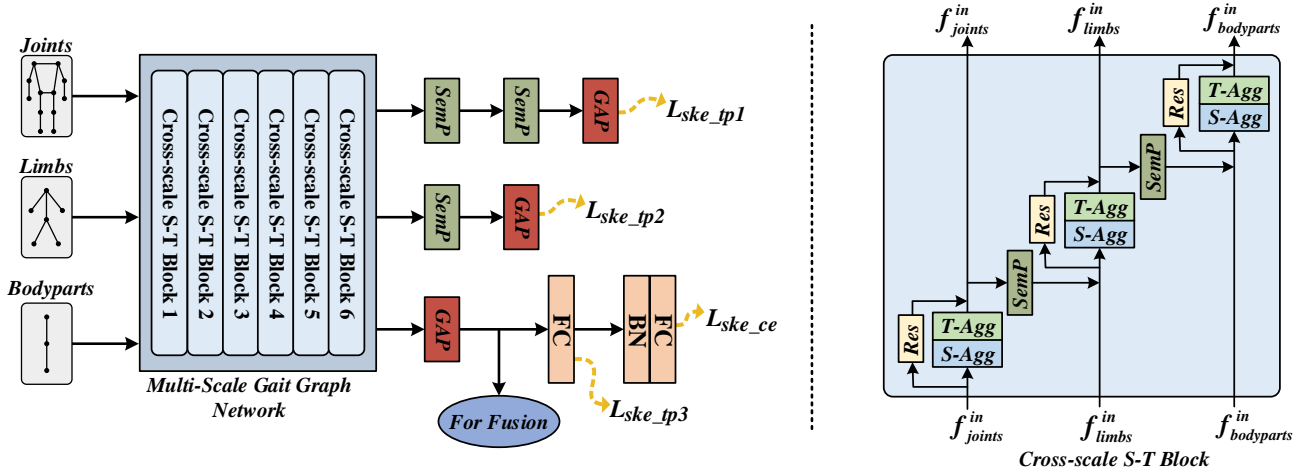


Fig. 5. The overall architecture of the proposed *multi-scale gait graph (MSGG)* network. *S-T* is short for Spatial-Temporal and *SemP* is short for Semantic Pooling. *GAP* denotes for the global pooling operation on the embeddings of all nodes to get an entire graph representation. *BN* for *Batch Normalization* and *FC* for the *Fully Connected Layer*. *S-Agg* denotes for the spatial information aggregation defined by Eq. 5 and *T-Agg* denotes for the temporal information aggregation defined by Eq. 7. *Res* for the residual connection.

partitioning strategy to implement the mapping function l_{ti} . As shown in Fig. 4, joints with larger amplitudes of movement can retain the gait periodicity better from the analysis of the temporal changes in skeleton data. Therefore, we propose to partition the neighbor set $N(v_{ti})$ based on the moving amplitudes of each neighbor node v_{tj} , formulated as:

$$l_{ti}(v_{tj}) = \begin{cases} 0, & \text{if } i = j; \\ 1, & \text{if } v_{tj} \in \text{Positive}; \\ 2, & \text{if } v_{tj} \in \text{Negative}. \end{cases} \quad (6)$$

where nodes with larger amplitudes of movement are regarded as *Positive* and nodes with smaller moving amplitudes are regarded as *Negative*², except for the current node v_{ti} . We name this strategy as *Gait temporal partitioning* and demonstrate its superiority in Sec.IV-D through the comparison with different partition strategies proposed in the ST-GCN [28]. Different strategies are clearly illustrated in Fig. 3 (b)-(e).

(a2) *Edge Importance Weighting*. To find out the contribution of different nodes in the k -th subset of the neighbor set $N(v_{ti})$, we add a learnable edge importance weight matrix W_E for the spatial graph convolution. It is straightforward to implement the edge importance weighting by substituting the matrix $(A_k + I)$ in Eq. 5 with $(A_k + I) \otimes W_E$, where \otimes denotes the Hadamard product.

(b) *Temporal Information Aggregation*. The well-ordered temporal axis of each node enables the MSGG to simply aggregate the temporal information within adjacent Γ frames rooted at v_{ti} as:

$$f_{out}^{t,i} = \left[f_{in}^{t-\lceil \Gamma/2 \rceil, i}, \dots, f_{in}^{t,i}, \dots, f_{in}^{t+\lceil \Gamma/2 \rceil, i} \right] W_{\Gamma \times 1}^i \quad (7)$$

where $f_{in}^{t,i}$ denotes the input feature vector of node v_{ti} . The learnable weight matrix $W_{\Gamma \times 1}^i$ is employed to aggregate the temporal information of adjacent Γ frames for node v_{ti} .

²*Positive*: right elbow, right knee, left elbow, left knee, right wrist, right ankle, left wrist, and left ankle. *Negative*: right shoulder, right hip, left shoulder, left hip. *Positive* and *Negative* nodes of the limbs spatial-temporal graph and the bodyparts spatial-temporal graph are similarly defined.

Multi-scale Gait Graph Network. The proposed *Multi-scale Gait Graph (MSGG)* network is built on the pyramid spatial-temporal graph constructed in Sec. III-B. Benefitting from the natural hierarchical structure defined by semantics, MSGG is able to exploit diverse multi-scale features and aggregate the information in a hierarchical way. As shown in Fig.5, the proposed MSGG consists of 3 branches that are conducted on the joints, the limbs, and the bodyparts spatial-temporal subgraph respectively. In MSGG, there are 6 Cross-scale Spatial-Temporal (S-T) Blocks, and each block completes the spatial-temporal information aggregation within each subgraph and the message passing across subgraphs.

The detailed structure of the Cross-scale S-T Block is shown in the right half of Fig. 5. The spatial-temporal information aggregation on each subgraph within a Cross-scale S-T Block is implemented by the execution of a spatial information aggregation (Eq. 5) and a temporal information aggregation (Eq. 7). To alleviate the problem of gradient vanishing, a residual connection is added to the spatial-temporal information aggregation except for the first Cross-scale S-T Block. Every time the spatial-temporal information aggregation has been done, the Cross-scale S-T Block will pass messages from the graph with lower semantic-level to the adjacent graph with higher semantic-level, i.e., from the joints subgraph to the limbs subgraph and from the limbs subgraph to the bodyparts subgraph, denoted as the *SemP* in Fig. 5.

Semantic Pooling. We name the message passing between adjacent subgraphs as the *Semantic Pooling (SemP)*. The goal of the *SemP* is to deliver the information from the graph with lower semantics to the graph with higher semantics. Given the mapping M between adjacent subgraphs, the message passing is formulated as:

$$f_{out}^{ti} = f_{in}^{ti} + \text{SemP}(f_{in}^{ta'}, f_{in}^{tb'}), ((a,b) \rightarrow i) \in M \quad (8)$$

where $f_{in}^{ta'}$ and $f_{in}^{tb'}$ denote the feature vector of v_{ta} and v_{tb} in the joints (limbs) subgraph, and f_{in}^{ti} denotes the feature vector of v_{ti} in the limbs (bodyparts) subgraph. Element $((a,b) \rightarrow i)$

in M denotes that the node v_{ta} and the node v_{tb} in a lower semantic graph are defined to be mapped to the node v_{ti} in the current graph. The mapping M between adjacent subgraphs is clearly illustrated in Fig. 3 (a). For simplicity, we use the *average*(\cdot) function as the implementation of *SemP*.

C. Bimodal Fusion Network

The proposed bimodal fusion network exploits complementary strengths of the two data modalities, i.e., silhouettes and skeletons, for gait recognition. As shown in Fig. 2, given N silhouette part features generated from the GaitPart module and the compact skeleton features extracted from the MSGG module followed by a Compact Block, the part-based bimodal fusion (the function $Fuse_n$ in Eq. 3) is implemented with the feature concatenation followed by a fully connected layer. We concatenate the skeleton sequence features reduced by the Compact Block [13] after each part-based silhouette sequence features and employ the fully connected layer (FC) to get the bimodal fusion for each part. This way of feature-level fusion is expected to extract specialized information from the skeleton data modality for the corresponding part features captured by the silhouette data modality. Therefore, a more comprehensive representation for gait recognition is obtained.

IV. EXPERIMENTS

The skeleton data is required for the proposed bimodal fusion network. In this case, empirical experiments are conducted on two public available gait datasets: CASIA-B and OUMVLP. For each dataset, we evaluate the performance of MSGG among skeleton-based methods and compare the bimodal fusion network with previous SOTA methods. Further ablation studies are conducted on CASIA-B.

A. Datasets

CASIA-B [38] is a popular gait dataset widely used in the research community. It contains 124 subjects where each subject has 10 walkings under three different conditions, i.e., 6 walkings in normal (NM), 2 walkings with a bag (BG), and 2 walkings in different clothes (CL). Each walking is recorded by 11 cameras located at different views simultaneously. The views for setting 11 cameras are uniformly distributed in $[0^\circ, 180^\circ]$ at an interval of 18° . In total, there are $(6 + 2 + 2) \times 11 = 110$ walking sequences per subject. Our experiments take the first 74 subjects as the training set and the rest 50 as the testing set. For evaluation, the first 4 normal walking sequences of each subject are regarded as the gallery and the rest are regarded as the probe.

OUMVLP [39] is a large public gait dataset that released only the silhouette data at the beginning. Recently, the skeleton data of OUMVLP estimated by AlphaPose [40] and Openpose [17] have been released by An et al. [26], named as the OUMVLP-Pose dataset. Therefore, the OUMVLP is an open-source dataset that has released both the silhouette data [39] and the skeleton data [26]. It contains 10307 subjects, 14 views ($[0^\circ, 90^\circ]$ and $[180^\circ, 270^\circ]$ at an interval of 15°) per subject, and 2 walking sequences (#00-01) per view. The division of

the training set and the testing set provided in OUMVLP [39] is quite different from that in OUMVLP-Pose [26]. For the comparison with previous SOTA methods, main experiments are conducted under the division provided in OUMVLP [39]. The 10307 subjects are divided into two disjoint groups: 5153 training and 5154 testing subjects. For evaluation, sequences #01 are kept in the gallery and sequences #00 are regarded as the probe.

B. Implementation Details

All models are implemented with PyTorch [41] and trained with NVIDIA Titan-V GPUs.

Input The silhouettes are pre-processed into the resolution of 64×64 using the methods described in [11]. Both the *Openpose* [17] and the *HRNet* [18] are applied in CASIA-B for pose estimation. For OUMVLP-Pose [26], we conduct experiments on the released AlphaPose dataset. As shown in Fig. 3 (a), 12 keypoints of the limbs and torso are used in this work. The number of subjects, the number of sequences per subject, and the number of frames per sequence in a mini-batch are set to (8, 16, 30) for CASIA-B, (32, 16, 30) for OUMVLP silhouettes, and (32, 16, 18) for OUMVLP skeletons.

Network We use the settings in GaitPart [12] for the silhouette module of our bimodal fusion network. There are 6 Cross-scale Spatial-Temporal Blocks in the proposed *Multi-scale Gait Graph (MSGG) network*. We set the number of channels in the first two blocks, the second two blocks, and the third two blocks as (16, 32, 64) for CASIA-B and (32, 64, 128) for OUMVLP. The dropping ratio of the *Dropout* layer and the output dimension of the *FC* layer in the Compact Block are set to (0.3, 32) for CASIA-B and (0.65, 32) for OUMVLP. The output dimension of each fused part features is set to 128 for CASIA-B and 256 for OUMVLP.

Loss The cross-entropy loss and Batch All (BA_+) triplet loss [42] are applied to train the network. The margin threshold m for triplet loss is set to 0.2. The triplet loss L_{sil_tp} is employed for pretraining the GaitPart module. And the loss L_{MSGG} for pretraining the MSGG module is computed as:

$$L_{MSGG} = \alpha L_{ske_tp1} + \beta L_{ske_tp2} + \gamma L_{ske_tp} + L_{ske_ce} \quad (9)$$

where L_{ske_tp1} , L_{ske_tp2} , and L_{ske_tp} are triplet losses calculated at the *joints*, the *limbs*, and the *bodyparts* branches respectively. L_{ske_ce} denotes the cross-entropy loss added after *FC* at the *bodyparts* branch. The α , β , and γ are set to 3, 2, and 1 respectively. And the total loss for the global training is computed as:

$$L = L_{sil_tp} + L_{ske_tp} + L_{ske_ce} \quad (10)$$

Optimizer The silhouette-based GaitPart module is pre-trained as in [12]. The SGD optimizer with momentum is adopted for MSGG pretraining and global training. In the pretraining of the MSGG, the learning rate is set to 0.1 and will be scaled to its 1/10 per 25K iterations for CASIA-B (per 75K iterations for OUMVLP) three times until convergence. In global training, the learning rate for the GaitPart module and the MSGG module is set to $1e-4$, and for the rest is set to 0.1. The learning rate will be scaled to its 1/10 per

TABLE I

THE RANK-1 ACCURACY (%) ON CAISA-B ACROSS DIFFERENT VIEWS, EXCLUDING THE IDENTICAL-VIEW CASES. BASED ON THE WALKING CONDITION, PROBE SEQUENCES ARE GROUPED INTO THREE SUBSETS, I.E., NM, BG, AND CL. THE 3D POSE [36] TAKES THE 2D POSES ESTIMATED BY OPENPOSE [17] AS INPUT. BIFUSION STANDS FOR THE PROPOSED BIMODAL FUSION NETWORK.

Gallery NM		0° – 180°												mean
Probe	Methods	0°	18°	36°	54°	72°	90°	108°	126°	144°	162°	180°		
NM	PoseGait [14] (3D Pose)	55.3	69.6	73.9	75.0	68.0	68.2	71.1	72.9	76.1	70.4	55.4	68.7	
	GaitGraph [16] (HRNet)	85.3	88.5	91.0	92.5	87.2	86.5	88.4	89.2	87.9	85.9	81.9	87.7	
	MSGG(ours, Openpose)	74.3	84.3	85.2	85.8	85.2	83.2	86.4	87.3	87.7	84.6	81.9	84.2	
	MSGG(ours, HRNet)	88.8	92.6	94.2	94.0	93.0	93.9	92.3	94.5	94.4	94.9	90.9	93.0	
	CNN-Ensemble [37]	88.7	95.1	98.2	96.4	94.1	91.5	93.9	97.5	98.4	95.8	85.6	94.1	
	GaitNet [7]	93.1	92.6	90.8	92.4	87.6	95.1	94.2	95.8	92.6	90.4	90.2	92.3	
	GaitSet [11]	90.8	97.9	99.4	96.9	93.6	91.7	95.0	97.8	98.9	96.8	85.8	95.0	
	GaitPart [12]	94.1	98.6	99.3	98.5	94.0	92.3	95.9	98.4	99.2	97.8	90.4	96.2	
	GaitGL [25]	96.0	98.3	99.0	97.9	96.9	95.4	97.0	98.9	99.3	98.8	94.0	97.4	
	silhouette-module(base)	93.4	98.0	99.1	97.5	94.1	91.9	96.4	97.6	99.0	97.9	91.9	96.1	
	BiFusion(ours, Openpose)	97.6	99.2	99.2	99.0	97.7	95.8	97.9	98.6	99.2	99.6	96.2	98.2	
	BiFusion(ours, HRNet)	98.0	99.1	99.5	99.3	98.7	97.5	98.5	99.1	99.6	99.5	96.8	98.7	
BG	PoseGait [14] (3D Pose)	35.3	47.2	52.4	46.9	45.5	43.9	46.1	48.1	49.4	43.6	31.1	44.5	
	GaitGraph [16] (HRNet)	75.8	76.7	75.9	76.1	71.4	73.9	78.0	74.7	75.4	75.4	69.2	74.8	
	MSGG(ours, Openpose)	59.9	65.8	70.3	69.2	67.6	66.8	65.9	68.0	69.8	66.8	63.0	66.6	
	MSGG(ours, HRNet)	77.9	81.3	81.7	80.2	78.2	73.8	76.5	77.0	78.6	80.5	73.0	78.1	
	CNN-LB [37]	64.2	80.6	82.7	76.9	64.8	63.1	68.0	76.9	82.2	75.4	61.3	72.4	
	GaitNet [7]	88.8	88.7	88.7	94.3	85.4	92.7	91.1	92.6	84.9	84.4	86.7	88.9	
	GaitSet [11]	83.8	91.2	91.8	88.8	83.3	81.0	84.1	90.0	92.2	94.4	79.0	87.2	
	GaitPart [12]	89.1	94.8	96.7	95.1	88.3	84.9	89.0	93.5	96.1	93.8	85.8	91.5	
	GaitGL [25]	92.6	96.6	96.8	95.5	93.5	89.3	92.2	96.5	98.2	96.9	91.5	94.5	
	silhouette-module(base)	90.1	95.8	96.0	93.6	88.0	84.4	88.1	93.4	96.0	93.7	86.0	91.4	
	BiFusion(ours, Openpose)	96.3	98.0	97.8	96.6	93.6	90.0	93.4	96.0	98.1	98.6	92.0	95.5	
	BiFusion(ours, HRNet)	95.8	97.9	98.2	97.6	94.4	91.6	93.9	96.6	98.5	98.3	93.1	96.0	
CL	PoseGait [14] (3D Pose)	24.3	29.7	41.3	38.8	38.2	38.5	41.6	44.9	42.2	33.4	22.5	36.0	
	GaitGraph [16] (HRNet)	69.6	66.1	68.8	67.2	64.5	62.0	69.5	65.6	65.7	66.1	64.3	66.3	
	MSGG(ours, Openpose)	46.5	54.9	55.2	54.7	54.7	57.3	57.3	58.3	61.3	59.6	54.6	55.9	
	MSGG(ours, HRNet)	62.2	67.4	66.2	70.2	68.8	66.2	67.4	69.2	71.1	73.4	69.7	68.3	
	CNN-LB [37]	37.7	57.2	66.6	61.1	55.2	54.6	55.2	59.1	58.9	48.8	39.4	54.0	
	GaitNet [7]	50.1	60.7	72.4	72.1	74.6	78.4	70.3	68.2	53.5	44.1	40.8	62.3	
	GaitSet [11]	61.4	75.4	80.7	77.3	72.1	70.1	71.5	73.5	73.5	68.4	50.0	70.4	
	GaitPart [12]	70.7	85.5	86.9	83.3	77.1	72.5	76.9	82.2	83.8	80.2	66.5	78.7	
	GaitGL [25]	76.6	90.0	90.3	87.1	84.5	79.0	84.1	87.0	87.3	84.4	69.5	83.6	
	silhouette-module(base)	75.1	84.9	87.4	82.3	77.2	74.8	79.6	83.8	83.7	80.3	65.8	79.5	
	BiFusion(ours, Openpose)	85.1	92.6	93.8	92.0	87.8	86.5	89.8	91.6	92.0	92.0	82.5	89.6	
	BiFusion(ours, HRNet)	88.7	93.9	95.6	93.8	91.4	89.4	92.3	93.8	94.2	93.7	86.2	92.1	

2K iterations for CASIA-B (per 4K iterations for OUMVLP) four times until convergence. We use $momentum = 0.9$ and $weight\ decay = 5e-4$ for the optimization. It is worth noting that all the experiments in this paper did not use any additional data other than the current dataset.

Testing Given a query Q , the goal is to retrieve all the samples with the same identity in gallery set \mathbb{G} . The Q is fed into the proposed bimodal fusion network to generate multiple part-based features $\{F_Q^1, F_Q^2, \dots, F_Q^N\}$. And the same process is applied on each sample G in gallery \mathbb{G} to obtain multiple part-based features $\{F_G^1, F_G^2, \dots, F_G^N\}$. We measure the similarity between Q and G by calculating the averaged Euclidean distance as $\frac{1}{N} \sum_{n=1}^N \|F_Q^n - F_G^n\|$.

C. Main Results

CASIA-B In the testing phase of CASIA-B, the probe sequences are grouped into three subsets, i.e., NM, BG, and CL. The evaluation is performed on each subset separately. All the results are averaged on gallery views excluding the identical-view cases.

Table I shows the performance comparison on CASIA-B for both the MSGG module and the bimodal fusion network. As listed in the first block of different probes, we compare the MSGG with PoseGait [14] and GaitGraph [16], where only the estimated skeleton data is taken as input. Although the GaitGraph performs better at few views in BG and CL, mean accuracies at different probes show the superiority of the proposed MSGG module over other skeleton-based methods under the same 2D pose estimation method (3D Pose used in PoseGait is based on Openpose). Besides, with the high-quality skeleton data provided by HRNet [18], MSGG obtains impressive results (NM-93.0%, BG-78.1%, CL-68.3%) on CASIA-B for skeleton-based gait recognition. The second and the third blocks of different probes in Table I show the performance comparison on CASIA-B for our bimodal fusion network. Taking advantage of the well-preserved body structure information in skeleton data, the bimodal fusion network reaches new SOTA performance on CASIA-B (NM-98.7%, BG-96.0%, CL-92.1%). Under the most challenging condition of walking in different clothes, the proposed method

TABLE II
THE RANK-1 ACCURACY (%) ON OUMVLP ACROSS DIFFERENT VIEWS, EXCLUDING THE IDENTICAL-VIEW CASES.

Gallery #01, Probe #00	Probe View														mean
Methods	0°	15°	30°	45°	60°	75°	90°	180°	195°	210°	225°	240°	255°	270°	
ST-GCN [28]	24.3	34.9	39.8	42.1	41.5	38.5	33.3	23.0	27.0	25.7	35.6	35.3	32.5	28.2	33.0
MSGG(ours)	43.8	58.8	64.0	66.4	65.9	62.9	57.8	40.6	48.4	44.4	60.6	60.3	56.6	51.8	55.9
GaitSet [11]	79.5	87.9	89.9	90.2	88.1	88.7	87.8	81.7	86.7	89.0	89.3	87.2	87.8	86.2	87.1
GaitPart [12]	82.6	88.9	90.8	91.0	89.7	89.9	89.5	85.2	88.1	90.0	90.1	89.0	89.1	88.2	88.7
GLN [13]	83.8	90.0	91.0	91.2	90.3	90.0	89.4	85.3	89.1	90.5	90.6	89.6	89.3	88.5	89.2
GaitGL [25]	84.9	90.2	91.1	91.5	91.1	90.8	90.3	88.5	88.6	90.3	90.4	89.6	89.5	88.8	89.7
silhouette-module(base)	82.57	88.93	90.84	91.00	89.75	89.91	89.50	85.19	88.09	90.02	90.15	89.03	89.10	88.24	88.74
BiFusion(ours)	86.17	90.60	91.28	91.56	90.88	90.78	90.48	87.76	89.48	90.38	90.65	89.95	89.82	89.32	89.94

TABLE III
ABLATION EXPERIMENTS CONDUCTED ON CASIA-B FOR THE PROPOSED MSGG. RESULTS ARE REPORTED IN THE RANK-1 ACCURACY (%) AVERAGED ON ALL 11 VIEWS, EXCLUDING THE IDENTICAL-VIEW CASES.

Partition Strategy	Pyramid Structure	Probes		
		NM	BG	CL
Uni-labeling	Joints+Limbs+Bodyparts	92.7	77.8	64.3
Distance	Joints+Limbs+Bodyparts	92.1	74.4	63.0
Spatial	Joints+Limbs+Bodyparts	90.0	71.7	62.7
Gait Temporal	Joints+Limbs+Bodyparts	93.0	78.1	68.3
Gait Temporal	Joints+Limbs	91.1	75.1	66.2
Gait Temporal	Joints	89.2	72.2	68.4
Gait Temporal	Joints+Joints+Joints	82.8	63.0	59.0
Gait Temporal	Joints+Limbs+Bodyparts (Separate)	90.9	72.8	58.6

improves the rank-1 accuracy on GaitGL [25] by 8.5%. This improvement shows the great potential of utilizing the natural advantages of skeletons to obtain the robustness to cloth changing for gait recognition.

OUMVLP The performance comparison on OUMVLP is shown in Table II. Since the division provided in OUMVLP [39] is not consistent with that in OUMVLP-Pose [26], we conduct the experiment on ST-GCN (baseline) for the comparison with the proposed MSGG network. As shown in Table II, the MSGG achieves better results under all the probe views, which demonstrates its effectiveness for the skeleton-based gait recognition. Furthermore, the proposed bimodal fusion network improves the mean accuracy on its silhouette module by 1.2%. This is less compared to the improvements in CASIA-B. Considering that the major improvements in CASIA-B are made on CL, the OUMVLP only contains walkings in normal and this may lead to less improvement. Besides, given the gap between OpenPose and HRNet for both the MSGG and the bimodal fusion in Table I, the poor performance of the AlphaPose [40] and the small number of frames of a sequence (roughly averaged at 25) in OUMVLP-Pose may bring negative effects.

D. Ablation Study

Ablation experiments are conducted on CASIA-B to analyze different components of the proposed network. Experimental settings are the same as those described in Sec. III.

Impact of the node partition strategy The first 4 rows in Table III compare the performance of different node partition

strategies, where three of them are directly taken from the ST-GCN [28]. The proposed *Gait temporal partitioning* strategy improves the accuracy on CASIA-B by at least +0.3% for NM, +0.3% for BG, and +4.0% for CL.

Impact of the pyramid structure The last 5 rows in Table III show the effectiveness of the proposed pyramid structure. In MSGG, there are three branches conducted on three spatial-temporal subgraphs respectively, corresponding to three different scales. The experimental results of the first branch (Joints), the first two branches (Joints+Limbs), and the whole MSGG (Joints+Limbs+Bodyparts) are listed in lines 4, 5, and 6 respectively. It can be seen that the accuracies are constantly improved with the increasing number of branches for both NM (+3.8%) and BG (+5.9%). Secondly, the results in the 7th row are the performance of the network with three joints branches. Except that the three branches are conducted on the joints spatial-temporal subgraph, the experimental settings of the 7th row are consistent with that of the 4th row. Therefore, the comparison of the 4th row and the 7th row demonstrates the effectiveness of the proposed multi-scale skeleton structure. Moreover, we conduct the experiment that turns off the message passing across different scales, i.e., removes the Semantic Pooling operation in the Cross-scale Spatial-Temporal Block, and concatenates the features of different scales (branches) for recognition. Comparing the results in the 4th row with that in the last row, the cross-scale message passing in MSGG improves the rank-1 accuracy by +2.1% for NM, +5.3% for BG, and +9.7% for CL.

Impact of the bimodal fusion The third block of different probes in Table I compares the mean accuracies of the bimodal fusion with that of its silhouette module (GaitPart). The effectiveness of utilizing the complementary strengths in different modalities for gait recognition is empirically studied. Compared with the silhouette-based GaitPart module, the bimodal fusion network improves the rank-1 accuracy by +2.6% for NM, +4.6% for BG, and +12.6% for CL.

V. CONCLUSION

In this work, the inherent hierarchical semantics of body joints in a skeleton is leveraged to design a novel *Multi-scale Gait Graph (MSGG)* network for the skeleton-based gait recognition. Furthermore, we propose a *bimodal fusion (BiFusion)* network to exploit the complementary strengths of the two data modalities, i.e., silhouettes and skeletons, for

gait identification. Extensive experiments on CASIA-B and OUMVLP demonstrate both the superiority of the proposed MSGG network among skeleton-based methods and the effectiveness of the bimodal fusion for gait recognition. The flexibility of the GCN-based gait recognition opens up many possible directions for future works on skeleton data, e.g. automatical node partitioning and hierarchy constructing. And the way to reach a more comprehensive representation for gait can be further explored.

REFERENCES

- [1] Z. Zhang, L. Tran, X. Yin, Y. Atoum, X. Liu, J. Wan, and N. Wang, "Gait recognition via disentangled representation learning," in *Proceedings of the IEEE/CVF Conference on Computer Vision and Pattern Recognition*, 2019, pp. 4710–4719.
- [2] Y. Sun, X. Wang, and X. Tang, "Deep learning face representation by joint identification-verification," *Advances in neural information processing systems*, vol. 27, 2014.
- [3] D. Maltoni, D. Maio, A. Jain, and S. Prabhakar, "Handbook of fingerprint recognition," *Ch Synthetic Fingerprint Generation*, vol. 33, no. 5-6, p. 1314, 2005.
- [4] Wildes and R.P., "Iris recognition: an emerging biometric technology," *Proceedings of the IEEE*, vol. 85, no. 9, pp. 1348–1363, 1997.
- [5] P. K. Larsen, E. B. Simonsen, and N. Lynnerup, "Gait analysis in forensic medicine," *Journal of Forensic Sciences*, vol. 53, no. 5, pp. 1149–1153, 2008.
- [6] I. Bouchrika, M. Goffredo, J. Carter, and M. Nixon, "On using gait in forensic biometrics," *Journal of forensic sciences*, vol. 56, no. 4, pp. 882–889, 2011.
- [7] Z. Zhang, L. Tran, F. Liu, and X. Liu, "On learning disentangled representations for gait recognition," *IEEE Transactions on Pattern Analysis and Machine Intelligence*, 2020.
- [8] X. Li, Y. Makihara, C. Xu, Y. Yagi, S. Yu, and M. Ren, "End-to-end Model-based Gait Recognition," in *Proceedings of the Asian Conference on Computer Vision*, 2020, pp. 3–20.
- [9] Y. Wang, X. Zhang, Y. Shen, B. Du, G. Zhao, L. C. C. Lizhen, and H. Wen, "Event-stream representation for human gaits identification using deep neural networks," *IEEE Transactions on Pattern Analysis and Machine Intelligence*, 2021.
- [10] G. Gallego, T. Delbruck, G. M. Orchard, C. Bartolozzi, B. Taba, A. Censi, S. Leutenegger, A. Davison, J. Conradt, K. Daniilidis *et al.*, "Event-based vision: A survey," *IEEE Transactions on Pattern Analysis and Machine Intelligence*, 2020.
- [11] H. Chao, Y. He, J. Zhang, and J. Feng, "Gaitset: Regarding gait as a set for cross-view gait recognition," in *Proceedings of the AAAI conference on artificial intelligence*, vol. 33, 2019, pp. 8126–8133.
- [12] C. Fan, Y. Peng, C. Cao, X. Liu, S. Hou, J. Chi, Y. Huang, Q. Li, and Z. He, "Gaitpart: Temporal part-based model for gait recognition," in *2020 IEEE/CVF Conference on Computer Vision and Pattern Recognition (CVPR)*, 2020, pp. 14 225–14 233.
- [13] S. Hou, C. Cao, X. Liu, and Y. Huang, "Gait lateral network: Learning discriminative and compact representations for gait recognition," in *European Conference on Computer Vision*. Springer, 2020, pp. 382–398.
- [14] R. Liao, S. Yu, W. An, and Y. Huang, "A model-based gait recognition method with body pose and human prior knowledge," *Pattern Recognition*, vol. 98, p. 107069, 2020.
- [15] M. Mao and Y. Song, "Gait recognition based on 3d skeleton data and graph convolutional network," in *2020 IEEE International Joint Conference on Biometrics (IJCB)*, 2020.
- [16] T. Teepe, A. Khan, J. Gilg, F. Herzog, S. Hörmann, and G. Rigoll, "Gait-graph: Graph convolutional network for skeleton-based gait recognition," 2021.
- [17] Z. Cao, T. Simon, S.-E. Wei, and Y. Sheikh, "Realtime multi-person 2d pose estimation using part affinity fields," in *2017 IEEE Conference on Computer Vision and Pattern Recognition (CVPR)*. IEEE Computer Society, 2017, pp. 1302–1310.
- [18] K. Sun, B. Xiao, D. Liu, and J. Wang, "Deep high-resolution representation learning for human pose estimation," in *Proceedings of the IEEE/CVF Conference on Computer Vision and Pattern Recognition (CVPR)*, June 2019.
- [19] N. V. Boulgouris and X. Huang, "Gait recognition using hmms and dual discriminative observations for sub-dynamics analysis," *IEEE Transactions on Image Processing*, vol. 22, no. 9, pp. 3636–3647, 2013.
- [20] J. Han and B. Bhanu, "Individual recognition using gait energy image," *IEEE transactions on pattern analysis and machine intelligence*, vol. 28, no. 2, pp. 316–322, 2005.
- [21] N. Takemura, Y. Makihara, D. Muramatsu, T. Echigo, and Y. Yagi, "On input/output architectures for convolutional neural network-based cross-view gait recognition," *IEEE Transactions on Circuits and Systems for Video Technology*, vol. 29, no. 9, pp. 2708–2719, 2017.
- [22] X. Ben, C. Gong, P. Zhang, R. Yan, Q. Wu, and W. Meng, "Coupled bilinear discriminant projection for cross-view gait recognition," *IEEE Transactions on Circuits and Systems for Video Technology*, vol. 30, no. 3, pp. 734–747, 2019.
- [23] S. Tong, Y. Fu, X. Yue, and H. Ling, "Multi-view gait recognition based on a spatial-temporal deep neural network," *IEEE Access*, vol. 6, pp. 57 583–57 596, 2018.
- [24] B. Lin, S. Zhang, and F. Bao, "Gait recognition with multiple-temporal-scale 3d convolutional neural network," in *Proceedings of the 28th ACM International Conference on Multimedia*, 2020, pp. 3054–3062.
- [25] B. Lin, S. Zhang, and X. Yu, "Gait recognition via effective global-local feature representation and local temporal aggregation," in *Proceedings of the IEEE/CVF International Conference on Computer Vision*, 2021, pp. 14 648–14 656.
- [26] W. An, S. Yu, Y. Makihara, X. Wu, C. Xu, Y. Yu, R. Liao, and Y. Yagi, "Performance evaluation of model-based gait on multi-view very large population database with pose sequences," *IEEE Transactions on Biometrics, Behavior, and Identity Science*, vol. 2, no. 4, pp. 421–430, 2020.
- [27] K. Xu, X. Jiang, and T. Sun, "Gait identification based on human skeleton with pairwise graph convolutional network," in *2021 IEEE International Conference on Multimedia and Expo (ICME)*. IEEE, 2021, pp. 1–6.
- [28] S. Yan, Y. Xiong, and D. Lin, "Spatial temporal graph convolutional networks for skeleton-based action recognition," in *Thirty-second AAAI conference on artificial intelligence*, 2018.
- [29] J. Liu, Z.-J. Zha, W. Wu, K. Zheng, and Q. Sun, "Spatial-temporal correlation and topology learning for person re-identification in videos," in *Proceedings of the IEEE/CVF Conference on Computer Vision and Pattern Recognition*, 2021, pp. 4370–4379.
- [30] N. Bodla, J. Zheng, H. Xu, J.-C. Chen, C. Castillo, and R. Chellappa, "Deep heterogeneous feature fusion for template-based face recognition," in *2017 IEEE winter conference on applications of computer vision (WACV)*. IEEE, 2017, pp. 586–595.
- [31] Y. Xin, L. Kong, Z. Liu, C. Wang, H. Zhu, M. Gao, C. Zhao, and X. Xu, "Multimodal feature-level fusion for biometrics identification system on iomt platform," *IEEE Access*, vol. 6, pp. 21 418–21 426, 2018.
- [32] A. A. Ross and R. Govindarajan, "Feature level fusion of hand and face biometrics," in *Biometric technology for human identification II*, vol. 5779. International Society for Optics and Photonics, 2005, pp. 196–204.
- [33] M. Faundez-Zanuy, "Data fusion in biometrics," *IEEE Aerospace and Electronic Systems Magazine*, vol. 20, no. 1, pp. 34–38, 2005.
- [34] S. Shekhar, V. M. Patel, N. M. Nasrabadi, and R. Chellappa, "Joint sparse representation for robust multimodal biometrics recognition," *IEEE Transactions on Pattern Analysis and Machine Intelligence*, vol. 36, no. 1, pp. 113–126, 2014.
- [35] Y. Xin, L. Kong, Z. Liu, C. Wang, H. Zhu, M. Gao, C. Zhao, and X. Xu, "Multimodal feature-level fusion for biometrics identification system on iomt platform," *IEEE Access*, pp. 1–1, 2018.
- [36] C. Chen and D. Ramanan, "3d human pose estimation = 2d pose estimation + matching," in *2017 IEEE Conference on Computer Vision and Pattern Recognition (CVPR)*. IEEE Computer Society, July 2017, pp. 5759–5767.
- [37] Z. Wu, Y. Huang, L. Wang, X. Wang, and T. Tan, "A comprehensive study on cross-view gait based human identification with deep cnns," *IEEE Transactions on Pattern Analysis & Machine Intelligence*, vol. 39, no. 02, pp. 209–226, 2017.
- [38] S. Yu, D. Tan, and T. Tan, "A framework for evaluating the effect of view angle, clothing and carrying condition on gait recognition," in *18th International Conference on Pattern Recognition (ICPR 2006)*, 20-24 August 2006, Hong Kong, China, 2006.
- [39] N. Takemura, Y. Makihara, D. Muramatsu, T. Echigo, and Y. Yagi, "Multi-view large population gait dataset and its performance evaluation for cross-view gait recognition," *IPSI Transactions on Computer Vision and Applications*, vol. 10, no. 1, pp. 1–14, 2018.

- [40] H.-S. Fang, S. Xie, Y.-W. Tai, and C. Lu, "Rmpe: Regional multi-person pose estimation," in *Proceedings of the IEEE international conference on computer vision*, 2017, pp. 2334–2343.
- [41] A. Paszke, S. Gross, F. Massa, A. Lerer, J. Bradbury, G. Chanan, T. Killeen, Z. Lin, N. Gimelshein, L. Antiga, A. Desmaison, A. Kopf, E. Yang, Z. DeVito, M. Raison, A. Tejani, S. Chilamkurthy, B. Steiner, L. Fang, J. Bai, and S. Chintala, "Pytorch: An imperative style, high-performance deep learning library," in *Advances in Neural Information Processing Systems*, 2019, pp. 8026–8037.
- [42] A. Hermans, L. Beyer, and B. Leibe, "In defense of the triplet loss for person re-identification," 2017.



machine learning.

Yongzhen Huang received the B.E. degree from Huazhong University of Science and Technology in 2006, and the Ph.D. degree from Institute of Automation, Chinese Academy of Sciences in 2011. He is currently an Associate Professor with School of Artificial Intelligence, Beijing Normal University. He has published one book and more than 80 papers at international journals and conferences such as TPAMI, IJCV, TIP, TSMCB, TMM, TCSVT, CVPR, ICCV, ECCV, NIPS, AAAI. His research interests include pattern recognition, computer vision and

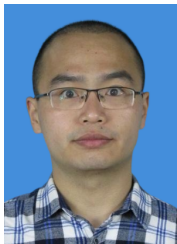


Yunjie Peng received her B.S. degree in the College of Computer and Information Science & College of Software from Southwest University, China, in 2018. She is currently a Ph.D. student in the School of Computer Science and Technology, Beihang University, China. Her research interests include gait recognition, computer vision, and machine learning.



Technology, Chinese Academy of Sciences and Beihang University.

Zhiqiang He is currently the Senior Vice President of Lenovo Company and President of Lenovo Capital and Incubator Group. This group is responsible for exploring external innovation as well as accelerating internal innovation for Lenovo Group, leveraging Lenovo global resources, power of capital, and entrepreneurship. Previously, he was the Chief Technology Officer and held various leadership positions in Lenovo, particularly in overseeing Lenovo's Research & Technology initiatives and systems. He is a doctoral supervisor at the Institute of Computing



Saihui Hou received the B.E. and Ph.D. degrees from University of Science and Technology of China in 2014 and 2019, respectively. He is currently an Assistant Professor with School of Artificial Intelligence, Beijing Normal University. His research interests include computer vision and machine learning. He recently focuses on gait recognition which aims to identify different people according to the walking patterns.



Kang Ma received his B.S. degree from the School of Electrical Engineering at Yanshan University, Qinhuangdao, China in 2016 and the M.S. degree from the School of Instrumentation and Optoelectronic Engine at Beihang University, Beijing, China in 2018. His current research interests include pattern recognition, computer vision, and machine learning.



Yang Zhang received his master's and Ph.D. degrees from Northumbria University, Newcastle upon Tyne, U.K. He is currently a senior researcher of Lenovo Research, Beijing. He has over thirty academic papers published on SCI journals and top conferences, and also has ten years research experience in computer vision, medical imaging, affective computing, and natural language processing.